Designed formation of hollow particle-based nitrogen-doped carbon nanofibers for high-performance supercapacitors

Chen, Li-Feng; Lu, Yan; Yu, Le; Lou, Xiong Wen (David)

2017

Chen, L.-F., Lu, Y., Yu, L., & Lou, X. W. (D.) (2017). Designed formation of hollow particle-based nitrogen-doped carbon nanofibers for high-performance supercapacitors. Energy & Environmental Science, 10(8), 1777-1783. doi:10.1039/C7EE00488E

https://hdl.handle.net/10356/82269

https://doi.org/10.1039/C7EE00488E

Broader context statement

Supercapacitors have been considered as one of the most promising electrochemical energy storage devices because of their high power density and long life span. Owing to the attractive physical and chemical properties including light weight, large surface area, good electrical conductivity, and good chemical stability, carbon materials have been regarded as the most important candidates as electrodes for supercapacitors. In the past decades, various efforts have been devoted to optimizing the electrochemical performance of carbon materials. Particularly, the design and synthesis of one-dimensional carbon hollow nanostructures are highly desirable due to their unique structural features. Moreover, introducing heteroatom dopants is also beneficial for enhancing the electrochemical activity. However, there are still some challenges for preparing high-performance electrodes using complex hollow nanostructured carbon materials with controllable compositions. In this present work, a facile electrospinning and carbonization method is designed to prepare hollow particle-based N-doped carbon nanofibers (HPCNFs-N). Benefiting from the hierarchical porous structure and high N-doping level, the obtained HPCNFs-N sample exhibits excellent electrochemical performance with remarkable specific capacitances at various current densities, high energy/power density and long-term cycling stability.

Designed formation of hollow particle-based nitrogen-doped carbon nanofibers for high-performance supercapacitors†

Li-Feng Chen, Yan Lu, Le Yu,* and Xiong Wen (David) Lou*

School of Chemical and Biomedical Engineering, Nanyang Technological University, 62 Nanyang Drive, Singapore 637459, Singapore

Email: yule0001@e.ntu.edu.sg; xwlou@ntu.edu.sg; davidlou88@gmail.com;

Web: http://www.ntu.edu.sg/home/xwlou/

† Electronic Supplementary Information (ESI) available: Additional morphology characterizations, XPS, BET data, electrochemical characterization of hollow particle-based nitrogen-doped carbon nanofibers and the control samples. See DOI: 10.1039/x0xx00000x

Carbon-based materials, as one of the most important electrode materials for supercapacitors, have attracted tremendous attention. At present, it is highly desirable but remains challenging to prepare one-dimensional carbon complex hollow nanomaterials for further improving the performance of supercapacitors. Herein, we report an effective strategy for the synthesis of hollow particle-based nitrogen-doped carbon nanofibers (HPCNFs-N). By embedding ultrafine zeolitic imidazolate framework (ZIF-8) nanoparticles into electrospun polyacrylonitrile (PAN), the as-prepared composite nanofibers are carbonized into hierarchical porous nanofibers composed of interconnected nitrogen-doped carbon hollow nanoparticles. Owing to the unique structural feature and the desirable chemical composition, the derived HPCNFs-N material exhibits much enhanced electrochemical properties as an electrode material for supercapacitors with remarkable specific capacitance at various current densities, high energy/power density and long cycling stability over 10000 cycles.

Introduction

Supercapacitors have been regarded as one of the most promising energy storage devices for next-generation electronics and electric vehicles owing to their high power density, fast charge/discharge rate and long cycle life.[1-4] The electrochemical properties of supercapacitors mainly depend on electrode materials.[5,6] Therefore, the development of advanced electrode materials has become a hot topic for the research in renewable energy-related fields. Among available candidates, carbonaceous materials are recognized as the most promising electrodes for supercapacitors because of their notable features including relatively light weight, high conductivity, high chemical stability, controllable porosity and plenty of active sites.[7-11]

In the past decades, various efforts have been devoted to optimizing the performance of carbon materials for supercapacitors. Particularly, the design and synthesis of one-dimensional (1D) carbon hollow nanostructures (i.e., carbon nanotubes) is highly desirable due to the apparent structural advantages as follows: (I) hollow structures guarantee the sufficient contact area between the active sites and the electrolyte;[8] (II) nano-sized subunits provide a reduced ion/electron diffusion path;[5] (III) the overall 1D features are believed to be beneficial for the electron transport.[12,13] Furthermore, introducing heteroatom dopants (N, P, B, S, etc.) is supposed to enhance the electrochemical activities by modifying the band gap and/or changing the surface characteristics.[14,15] Nevertheless, the energy/power density of hollow structures with simple configurations (i.e., single-shelled nanotubes) often suffers from low tapping density of the active materials.[16] Besides, the synthetic strategies for hollow structures usually require some expensive hard templates, which have to be removed by additional treatments.[17] Also, the doping processes need some hazardous chemical reactions.[18,19] These complex synthetic procedures largely hinder the practical applications of

carbon-based materials for supercapacitors.

To address these issues, we develop a facile electrospinning and carbonization method to prepare hollow particle-based N-doped carbon nanofibers (denoted as HPCNFs-N). ZIF-8 nanoparticles are first embedded into electrospun polyacrylonitrile (PAN) to form the PAN/ZIF-8 composite nanofibers. After a subsequent carbonization reaction, primary ZIF-8 nanoparticle subunits within PAN matrix are transformed into interconnected N-doped carbon hollow nanoparticles for constructing the hierarchical porous nanofibers. During the synthesis, the electrospinning method enables the formation of 1D composite precursor. Therefore, no redundant template-removal treatments are involved. Moreover, the large amount of N species within the organic ligands in ZIF-8 and PAN molecules is well-retained in the final product. Benefiting from the hierarchical porous structure and high N-doping level, these HPCNFs-N nanofibers exhibit excellent electrochemical performance with high specific capacitance, remarkable energy/power density and long-term cycling stability.

Results and discussion

The synthetic strategy for HPCNFs-N is schematically depicted in Fig. 1. In a typical procedure, ZIF-8 nanoparticles are first embedded into PAN nanofibers by an electrospinning method. After a heating treatment at 900 ^{o}C in inert atmosphere, the organic ligands in ZIF-8 and PAN molecules are decomposed and converted into N-doped carbon materials. Meanwhile, the Zn^{2+} species in ZIF-8 particles are reduced to metallic Zn, which further vaporizes at high temperature. The large mass loss within the interconnected ZIF-8 particles results in formation of the hierarchical porous nanofibers.

As revealed by the field-emission scanning electron microscopy (FESEM) observations (Fig. 2a and c), the as-prepared PAN/ZIF-8 composite nanofibers are very long and uniform in diameter (~1.4 μm). Compared with the electrospun PAN nanofibers without adding ZIF-8 particles (Fig. S1, see ESI†), the rough surface of the PAN/ZIF-8 sample indicates that the ZIF-8 nanoparticles are well dispersed within the whole nanofiber. The corresponding transmission electron microscopy (TEM) image (Fig. 2d) confirms the solid nature of the as-prepared PAN/ZIF-8 nanofibers. The XRD results also confirm the successful loading of ZIF-8 particles within the amorphous PAN nanofibers for the PAN/ZIF-8 sample (Fig. S2, see ESI†).

After the thermal treatment in N_2 gas, the resultant HPCNFs-N sample retains the fiber-like morphology without apparent changes in appearance (Fig. 3a and b). Benefitting from the entangled network formed by the electrospun PAN/ZIF-8 nanofibers, the obtained HPCNFs-N sample exhibits good flexibility (inset of Fig. 3a and Fig. S3, see ESI†). Magnified FESEM images (Fig. 3c and d) and TEM images (Fig. 3e and f) reveal that these nanofibers are composed of numerous hollow nanoparticles interconnected with each other. In addition, the confined carbonization process within the PAN matrix can prevent the carbonized ZIF-8 nanoparticles from agglomeration (Fig. S4, see ESI†). As shown by the high-resolution transmission electron microscope (HRTEM) examination (Fig. 3g), a distinct set of visible lattice fringes with an inter-planar spacing of ~0.35 nm can be clearly identified, corresponding to the *d*-spacing of (002) plane of graphitic carbon.[20,21] The existence of graphitic carbon might be beneficial to the electrical conductivity of HPCNFs-N. Furthermore, energy-filtered transmission electron microscope (EFTEM) mapping images based on an individual nanofiber demonstrate the uniform distribution of C and N elements within the entire porous structure (Fig. 3h-k). The effect of carbonization temperature on the structure of HPCNFs-N

is also investigated. When PAN/ZIF-8 is heated at the temperature of 800 ºC, the volume shrinkage for the achieved sample (denoted as HPCNFs-N-800) is reduced (Fig. S5a, see ESI†). As a result, the diameter of the HPCNFs-N-800 nanofibers is much larger than that of the HPCNFs-N product annealed at 900 ºC (Fig. S6, see ESI†). In comparison, the sample annealed at 1000 ºC (denoted as HPCNFs-N-1000) is rather compact (Fig. S5c, see ESI†) with a reduced diameter of the obtained nanofibers (Fig. S7, see ESI†). Besides, more broken hollow nanoparticles can be observed along the whole fiber.

Two broad peaks can be identified from X-ray powder diffraction (XRD) patterns (Fig. 4a) of HPCNFs-N and the control samples, confirming the crystalline nature of carbon with very small particle size.[22] Raman spectra further provide some information about the characteristic G and D bands of carbon species in the as-prepared nanofibers. As shown in Fig. 4b, the intensive peaks emerged at around 1338 and 1585 cm^{-1} are associated with the in-plane A_{1g} zone-edge mode (D band) and the doubly degenerate zone center E_{2g} mode (G band), respectively.[15,23,24] Meanwhile, the broad peak appearing in the 2500-3500 cm^{-1} region can be assigned to the second-order of D band (2D band).[25] According to the increased intensity ratio of the G to D bands (I_G/I_D), the graphenic order of carbon in the nanofibers is largely enhanced with the increase of carbonization temperature.

The chemical compositions of the HPCNFs-N sample are further investigated by electron energy-loss spectroscopy (EELS) measurement. Two visible edges in the EELS spectrum (Fig. 4c) starting at 279 and 395 eV are assigned to the characteristic K-shell ionization edges of C and N, respectively, indicating the co-existence of C and N in the sample.[26] The two bands clearly show a pre-peak corresponding to the 1s-π^* antibonding orbit, followed by a wider band related with the

1s-σ^* antibonding orbit. The well-defined π^* and σ^* features of C and N K-edge confirm that both C and N elements are sp^2 hybridized.[20,26,27] According to the EELS spectrum, the N/C ratio within the HPCNFs-N is approximately 0.091 (91.66±12.5 at.% C and 8.34±1.1 at.% N), consistent with the result from elemental analysis (78.43 wt.% C, 9.39 wt.% N and 1.15 wt.% H; the atomic ratio of N/C is 0.103). X-ray photoelectron spectroscopy (XPS) measurements are also conducted to further clarify the contents and types of N species in the samples. From XPS survey spectra (Fig. S8a), the atomic percentage of N in HPCNFs-N, HPCNFs-N-800 and HPCNFs-N-1000 is estimated to be around 7.85%, 12.05% and 3.63%, respectively. Besides, the atomic percentage of oxygen in HPCNFs-N-800, HPCNFs-N, and HPCNFs-N-1000 is 6.06%, 5.35%, and 4.94%, respectively. Moreover, there are no Zn species remaining for all the samples after the high temperature annealing and the subsequent acid treatment. Their N 1s region spectra (Fig. 4d and Fig. S8b and c, see ESI†) can be deconvoluted into four peaks, pyridinic N (N-6), pyrrolic/pyridonic N (N-5), quaternary N and oxidic N.[28,29] Among these types, N-5 and N-6 species are the dominant N-containing functional groups in HPCNFs-N, which serve as electrochemically active sites in various electrochemical applications.[30,31] Whereas, N-5 species are gradually converted to N-6 and inactive quaternary N species upon the increase of the carbonization temperature.

Pore characteristics of the samples are characterized through N_2 adsorption-desorption measurements. The remarkable hysteresis loop of type IV indicates that the HPCNFs-N sample exhibits a mesoporous structure (Fig. S9, see ESI†).[32] The corresponding pore-size-distribution (PSD) curve shows that the size of majority of the pores falls in the range of 3 to 4 nm. The detailed parameters about the Brunauer-Emmett-Teller (BET) specific surface area (S_{BET}) and pore volume are summarized in Table S1. It can be found that the S_{BET} of HPCNFs-N (417.9 $m^2\ g^{-1}$) is much

larger than that of the N-doped carbon (denoted as C-N) obtained by carbonizing ZIF-8 particles (223.1 $m^2 g^{-1}$, Fig. S10, see ESI†). Besides, the S_{BET} of the N-doped carbon nanofibers (denoted as N-CNFs) obtained by carbonizing the electrospun PAN nanofibers is very small. The above results demonstrate the importance of the introduction of ZIF-8 nanoparticles in the precursor to improve the specific surface area of HPCNFs-N.

Next, electrochemical performance of HPCNFs-N is assessed as electrodes for supercapacitors in a two-electrode cell configuration using an aqueous H_2SO_4 solution (2.0 M) as the electrolyte (Fig. S11, see ESI†). The typical cyclic voltammetry (CV) curves of HPCNFs-N at the sweep rates ranging from 2.0 to 100.0 mV s^{-1} are presented in Fig. 5a. The nearly rectangular shape suggests its classical capacitive behavior as the electrodes of electrical double layer supercapacitors,[33] where the small humps originate from Faradaic reactions of active functional groups on the HPCNFs-N surface. Moreover, the CV profiles over variable scan rates (up to 1500 mV s^{-1}; Fig. S12a, see ESI†) display quasi-rectangular shapes, suggesting its high-rate capability. In comparison, the control samples of C-N (Fig. S13a, see ESI†) and N-CNFs (Fig. S14, see ESI†) show similar rectangular CV curves with much reduced capacitance. This clearly verifies the importance of large surface area and desirable chemical composition for electrochemical performance.

Furthermore, the galvanostatic charge/discharge curves of HPCNFs-N (Fig. 5b and Fig. S12b, see ESI†) collected at various current densities from 1.0 to 200.0 A g^{-1} are nearly linear and symmetrical, which further confirms its capacitor-like feature and good electrochemical reversibility. The specific capacitance (C_s) as a function of the current density is calculated based on the discharge curves. As seen in Fig. 5c, the C_s of HPCNFs-N is as high as 307.2, 283.2, 264, 252.2 and 235.2 F g^{-1} at the discharge current density of 1.0, 2.0, 5.0, 10.0 and 20.0 A g^{-1}, respectively. This

suggests that about 76.6% of the capacitance is retained when the charge-discharge rate is increased from 1.0 to 20.0 A g^{-1}. Moreover, even at a much higher current density of 50.0 A g^{-1}, the C_s for HPCNFs-N still reaches a high value of 193.4 F g^{-1}. The variation of *IR* drop at different discharge current densities (Fig. S12c, see ESI†) reveals the supercapacitor device based on the HPCNFs-N electrodes has small internal resistance, which is beneficial for a high power discharge in practical applications. The remarkable performance of HPCNFs-N compares favorably to the behavior of many reported representative carbon materials (Table S2, see ESI†).[15,19,34-43] Although the control samples of HPCNFs-N-800, HPCNFs-N-1000 (Fig. S12d-f, see ESI†) and C-N (Fig. S13b, see ESI†) display similar electrochemical characteristics as capacitor-like electrodes, their electrochemical properties in terms of C_s values and/or rate performance are much inferior. Overall, these inspiring results might be attributed to the unique structural and compositional features of HPCNFs-N, such as high specific area, desirable pore size distribution and sufficient electrochemically active sites.

The power/energy density is key parameter for evaluating electrochemical performance of the electrode materials in supercapacitors.[37,38,44,45] The Ragone plots (Fig. S15, see ESI†) clearly illustrate that the supercapacitor device using the HPCNFs-N electrodes exhibits much enhanced energy/power density compared with the supercapacitors based on the control samples. Besides, the power/energy density of the device in our work is comparable to that of some other similar carbon-based supercapacitors.[15,38,40,42] Specifically, an energy density of as high as 10.96 Wh kg^{-1} can be achieved at a power density of 250 W kg^{-1}. Moreover, it still maintains 6.72 Wh kg^{-1} even at high power density of 25000 W kg^{-1}. Overall, the performance is competitive with that of some N-doped carbon-based supercapacitors.[15,37,38]

Lastly, the electrochemical stability of the supercapacitor is tested by continuous galvanostatic charge-discharge cycling at a current density of 5.0 A g^{-1}. As shown in Fig. 5d, the specific capacitance maintains 98.2% of initial value after 10000 cycles, indicating the excellent electrochemical stability of the supercapacitor device. The Coulombic efficiency keeps almost 100% after the first few cycles (Fig. S16, see ESI†). Furthermore, we study the morphology of electrodes after the repeated charge-discharge processes. As indicated by morphological observations, the integrity of the HPCNFs-N electrode is well preserved, confirming its superior structural stability (Fig. S17, see ESI†).

The above excellent electrochemical properties of HPCNFs-N might be ascribed to their unique structural and compositional features. First, the hierarchical porous structure composed of numerous interconnected carbon hollow nanoparticles guarantees sufficient electrochemical active sites, improved electrochemical kinetics and enhanced structural stability. Second, the unique 1D fiber-like architecture ensures the good ion/electron transport. Third, the high N-doping level might be beneficial for the electrochemical reactions by introducing functional groups and/or modifying the band gap.

Conclusions

In summary, we present an effective method for producing hollow particle-based N-doped carbon nanofibers *via* a simple carbonization treatment of electrospun ZIF-8/PAN composite precursor. With these hierarchical porous nanofibers as the electrodes, the as-assembled supercapacitor device exhibits remarkable supercapacitive performance with high specific capacitances at various current densities (307.2 F g^{-1} at 1.0 A g^{-1} and 193.4 F g^{-1} at 50.0 A g^{-1}), enhanced energy/power density (a

maximum energy density of 10.96 Wh kg^{-1} and power density of 25000 W kg^{-1}), and outstanding cycling stability with only 1.8% capacitance loss over 10000 cycles.

Experimental

Preparation of ZIF-8 particles

Typically, 1.487 g of $Zn(NO_3)_2 \cdot 6H_2O$ was dissolved in 100 mL of methanol. 3.284 g of 2-methylimidazole (MeIM) was dissolved into 50 mL of methanol. Then, the two solutions were rapidly mixed together under magnetic stirring at room temperature for 2 h. Next, the white powder was collected by centrifugation (10000 rpm, 3 min), washed several times with methanol, and dried at 80 °C for 12 h.

Preparation of hollow particle-based N-doped carbon nanofibers (HPCNFs-N)

0.263 g of as-synthesized ZIF-8 powder was dispersed in 2.063 g of dimethylformamide (DMF) solvent via sonicating for 30 min, followed with the addition 0.175 g of polyacrylonitrile (PAN, average MW 150000). The mixture was stirred for 24 h to form a homogeneously dispersed solution. Then, the mixture solution was loaded into a syringe (5 mL) with a stainless-steel nozzle, which was connected to a high-voltage power supply. The high voltage, feeding rate, temperature and distance between the anode and cathode are fixed at 20 kV, 1.0 mL h^{-1}, 35 °C and 18 cm, respectively. Then, the electrospun PAN/ZIF-8 was dried at 70 °C overnight in vacuum. Afterwards, the composite nanofibers were carbonized under the protection of N_2 gas through a two-stage heating process. Specifically, they were first heated at 550 °C for 1 h with a ramping rate of 2 °C min^{-1}, followed by a further thermal annealing at 900 °C for 2 h with a ramping rate of 5 °C min^{-1}. Subsequently, the resultant materials were washed thoroughly in a H_2SO_4 solution (3.0 M) to

remove residual Zn species. Finally, the as-obtained HPCNFs-N sample was rinsed with ethanol and deionized water and dried in vacuum at 80 ^{o}C.

The control sample of N-doped carbon nanofibers (N-CNFs) was synthesized by a similar procedure without adding ZIF-8 particles. For the other two samples of hollow particle-based N-doped carbon nanofibers annealed at 800 ^{o}C (denoted as HPCNFs-N-800) or 1000 ^{o}C (HPCNFs-N-1000), the PAN/ZIF-8 fiber was carbonized under the protection of N_2 gas through a two-stage heating process. They were first heated at 550 ^{o}C for 1 h with a ramping rate of 2 ^{o}C min^{-1}, followed by a further thermal annealing at 800 ^{o}C (or 1000 ^{o}C) for 2 h with a ramping rate of 5 ^{o}C min^{-1}.

Materials characterization

The morphology of the samples was examined using field-emission scanning electron microscope (FESEM; JEOL-6700F) and transmission electron microscope (TEM; JEOL, JEM-2010). High-resolution transmission electron microscope (HRTEM) images, energy filtered transmission electron microscope (EFTEM) mapping images and electron energy loss spectroscopy (EELS) spectra were collected on a JEM-ARM 200F atomic resolution analytical microscope. The crystal phase of the products was examined by X-ray diffraction (XRD; Bruker, D8-Aavance X-ray Diffractometer, Cu Kα radiation, λ = 1.5406 Å). Raman scattering spectra were collected on a confocal micro-Raman system (WITec alpha 300) at ambient conditions, using a diode laser (excitation wavelength is 532 nm). X-ray photoelectron spectroscopy (XPS) spectra were obtained on an ESCALab MKII X-ray photoelectron spectrometer with a Mg Kα (1253.6 eV) excitation source. Element analysis was carried out using a CNH analyzer (Elementarvario EL cube). N_2 adsorption/desorption isotherms were obtained on Quantachrome Instruments v4.01, and the

Barrett-Emmett-Teller (BET) theory was used for surface area calculations. Pore-size-distribution (PSD) plots were obtained from the adsorption branch of the isotherm using the Barrett-Joyner-Halenda (BJH) model.

Electrochemical measurements

All electrochemical measurements were carried out using a two-electrode system with a CHI 660D electrochemical workstation at room temperature. Before the assembly of the supercapacitors, the electrodes were soaked in an aqueous H_2SO_4 electrolyte (2.0 M) for 6 h. The employed two-electrode configuration consisted of two slices of electrode materials with the same size (1.0 cm × 1.0 cm), the filter paper (pore size: 225 nm) as separator, and a pair of Ti foil as the current collectors. Moreover, the whole supercapacitor device was wrapped with parafilm for fixation. The tap density of the supercapacitor electrode was estimated by direct mass and physical dimension measurements, which is about 0.27 g cm^{-3}. CV curves and galvanostatic charge/discharge measurements were recorded at the working voltage of 0.0 to 1.0 V. For the electrochemical performance of N-CNFs and C-N, the electrode slurry was prepared by mixing active material (80 wt.%), acetylene black (Super-P, 10 wt.%), and polyvinylidene fluoride (PVDF, 10 wt.%) in *N*-methyl-2-pyrrolidone. After spreading the above slurry on Ti foil (active material loading: ~1.0 mg cm^{-2}), the electrodes were dried at 80 °C for 24 h under vacuum.

The mass based specific capacitance (C_s) was calculated from the galvanostatic discharge process using the equations (1):

$$C_s = \frac{4I_{cons}}{mdV/dt} \quad (1)$$

where I_{cons} (A) corresponds to the constant discharge current, dV/dt (V/s) represents the slope of the discharge curve, and m (g) refers to the total mass of active material on the two electrodes,

respectively.

The energy density (E) and power density (P) of the supercapacitor device were calculated using the equations (2) and (3)

$$E = \frac{\frac{1}{8} \times C_s \times (\Delta V)^2 \times 1000}{3600} \quad (2)$$

$$P = \frac{E \times 3600}{\Delta t} \quad (3)$$

where E (Wh kg^{-1}) is the mass based energy density, ΔV (V) corresponds to the voltage window, P (W kg^{-1}) is the average power density and Δt (s) refers to the discharge time.

Acknowledgements

X. W. L. acknowledges the funding support from the National Research Foundation (NRF) of Singapore via the NRF investigatorship (NRF-NRFI2016-04) and Ministry of Education of Singapore through the AcRF Tier-2 funding (MOE2014-T2-1-058; ARC41/14).

Notes and references

1. P. Huang, C. Lethien, S. Pinaud, K. Brousse, R. Laloo, V. Turq, M. Respaud, A. Demortiere, B. Daffos, P. L. Taberna, B. Chaudret, Y. Gogotsi and P. Simon, *Science*, 2016, **351**, 691.
2. G. G. Eshetu, M. Armand, B. Scrosati and S. Passerini, *Angew. Chem., Int. Ed.*, 2014, **53**, 13342.
3. G. Q. Zhang and X. W. Lou, *Adv. Mater.*, 2013, **25**, 976.
4. S. J. Peng, L. L. Li, H. B. Wu, S. Madhavi and X. W. Lou, *Adv. Energy Mater.*, 2015, **5**, 1401172.
5. A. S. Arico, P. Bruce, B. Scrosati, J. M. Tarascon and W. Van Schalkwijk, *Nat. Mater.*, 2005, **4**, 366.
6. P. Simon and Y. Gogotsi, *Nat. Mater.*, 2008, **7**, 845.
7. L. L. Zhang and X. S. Zhao, *Chem. Soc. Rev.*, 2009, **38**, 2520.

8. J. L. Liu, L. L. Zhang, H. B. Wu, J. Y. Lin, Z. X. Shen and X. W. Lou, *Energy Environ. Sci.*, 2014, **7**, 3709.

9. D. Pech, M. Brunet, H. Durou, P. H. Huang, V. Mochalin, Y. Gogotsi, P. L. Taberna and P. Simon, *Nat. Nanotechnol.*, 2010, **5**, 651.

10. Y. Wang, Z. Q. Shi, Y. Huang, Y. F. Ma, C. Y. Wang, M. M. Chen and Y. S. Chen, *J. Phys. Chem. C*, 2009, **113**, 13103.

11. J. F. Chen, Y. L. Han, X. H. Kong, X. Z. Deng, H. J. Park, Y. L. Guo, S. Jin, Z. K. Qi, Z. Lee, Z. H. Qiao, R. S. Ruoff and H. X. Ji, *Angew. Chem., Int. Ed.*, 2016, **55**, 13822.

12. R. H. Baughman, A. A. Zakhidov and W. A. de Heer, *Science*, 2002, **297**, 787.

13. W. Li, F. Zhang, Y. Q. Dou, Z. X. Wu, H. J. Liu, X. F. Qian, D. Gu, Y. Y. Xia, B. Tu and D. Y. Zhao, *Adv. Energy Mater.*, 2011, **1**, 382.

14. F. B. Su, C. K. Poh, J. S. Chen, G. W. Xu, D. Wang, Q. Li, J. Y. Lin and X. W. Lou, *Energy Environ. Sci.*, 2011, **4**, 717.

15. L. F. Chen, Z. H. Huang, H. W. Liang, H. L. Gao and S. H. Yu, *Adv. Funct. Mater.*, 2014, **24**, 5104.

16. G. Q. Zhang, B. Y. Xia, C. Xiao, L. Yu, X. Wang, Y. Xie and X. W. Lou, *Angew. Chem., Int. Ed.*, 2013, **52**, 8643.

17. W. Zhang, Z. Y. Wu, H. L. Jiang and S. H. Yu, *J. Am. Chem. Soc.*, 2014, **136**, 14385.

18. L. Qie, W. M. Chen, H. H. Xu, X. Q. Xiong, Y. Jiang, F. Zou, X. L. Hu, Y. Xin, Z. L. Zhang and Y. H. Huang, *Energy Environ. Sci.*, 2013, **6**, 2497.

19. H. Zhu, J. Yin, X. L. Wang, H. Y. Wang and X. R. Yang, *Adv. Funct. Mater.*, 2013, **23**, 1305.

20. Y. C. Zhao, Z. Liu, W. G. Chu, L. Song, Z. X. Zhang, D. L. Yu, Y. J. Tian, S. S. Xie and L. F. Sun, *Adv. Mater.*, 2008, **20**, 1777.

21. D. Y. Chung, K. J. Lee, S. H. Yu, M. Kim, S. Y. Lee, O. H. Kim, H. J. Park and Y. E. Sung, *Adv. Energy Mater.*, 2015, **5**, 1401309.

22. F. C. Zheng, Y. Yang and Q. W. Chen, *Nat. Commun.*, 2014, **5**, 5261.

23. B. Y. Xia, Y. Yan, N. Li, H. B. Wu, X. W. Lou and X. Wang, *Nat. Energy*, 2016, **1**, 15006.

24. A. C. Ferrari, *Solid State Commun.*, 2007, **143**, 47.

25. H. J. Huang, S. B. Yang, R. Vajtai, X. Wang and P. M. Ajayan, *Adv. Mater.*, 2014, **26**, 5160.

26. L. Ci, L. Song, C. H. Jin, D. Jariwala, D. X. Wu, Y. J. Li, A. Srivastava, Z. F. Wang, K. Storr, L. Balicas, F. Liu and P. M. Ajayan, *Nat. Mater.*, 2010, **9**, 430.
27. R. R. Schlittler, J. W. Seo, J. K. Gimzewski, C. Durkan, M. S. M. Saifullah and M. E. Welland, *Science*, 2001, **292**, 1136.
28. D. H. Guo, R. Shibuya, C. Akiba, S. Saji, T. Kondo and J. Nakamura, *Science*, 2016, **351**, 361.
29. C. Young, R. R. Salunkhe, J. Tang, C. C. Hu, M. Shahabuddin, E. Yanmaz, M. S. A. Hossain, J. H. Kim and Y. Yamauchi, *Phys. Chem. Chem. Phys.*, 2016, **18**, 29308.
30. L. F. Chen, X. D. Zhang, H. W. Liang, M. G. Kong, Q. F. Guan, P. Chen, Z. Y. Wu and S. H. Yu, *ACS Nano*, 2012, **6**, 7092.
31. H. M. Jeong, J. W. Lee, W. H. Shin, Y. J. Choi, H. J. Shin, J. K. Kang and J. W. Choi, *Nano Lett.*, 2011, **11**, 2472.
32. J. Wei, D. D. Zhou, Z. K. Sun, Y. H. Deng, Y. Y. Xia and D. Y. Zhao, *Adv. Funct. Mater.*, 2013, **23**, 2322.
33. P. Simon, Y. Gogotsi and B. Dunn, *Science*, 2014, **343**, 1210.
34. J. Tang, R. R. Salunkhe, J. Liu, N. L. Torad, M. Imura, S. Furukawa and Y. Yamauchi, *J. Am. Chem. Soc.*, 2015, **137**, 1572.
35. H. L. Jiang, B. Liu, Y. Q. Lan, K. Kuratani, T. Akita, H. Shioyama, F. Q. Zong and Q. Xu, *J. Am. Chem. Soc.*, 2011, **133**, 11854.
36. F. F. Cao, M. T. Zhao, Y. F. Yu, B. Chen, Y. Huang, J. Yang, X. H. Cao, Q. P. Lu, X. Zhang, Z. C. Zhang, C. L. Tan and H. Zhang, *J. Am. Chem. Soc.*, 2016, **138**, 6924.
37. B. Li, F. Dai, Q. F. Xiao, L. Yang, J. M. Shen, C. M. Zhang and M. Cai, *Energy Environ. Sci.*, 2016, **9**, 102.
38. J. Zhao, H. W. Lai, Z. Y. Lyu, Y. F. Jiang, K. Xie, X. Z. Wang, Q. Wu, L. J. Yang, Z. Jin, Y. W. Ma, J. Liu and Z. Hu, *Adv. Mater.*, 2015, **27**, 3541.
39. N. P. Wickramaratne, J. T. Xu, M. Wang, L. Zhu, L. M. Dai and M. Jaroniec, *Chem. Mater.*, 2014, **26**, 2820.
40. Y. L. Cheng, L. Huang, X. Xiao, B. Yao, L. Y. Yuan, T. Q. Li, Z. M. Hu, B. Wang, J. Wan and J. Zhou, *Nano Energy*, 2015, **15**, 66.

41. C. H. Wang, C. Liu, J. S. Li, X. Y. Sun, J. Y. Shen, W. Q. Han and L. J. Wang, *Chem. Commun.*, 2017, **53**, 1751.

42. G. Y. Zhu, L. B. Ma, H. L. Lv, Y. Hu, T. Chen, R. P. Chen, J. Liang, X. Wang, Y. R. Wang, C. Z. Yan, Z. X. Tie, Z. Jin and J. Liu, *Nanoscale*, 2017, **9**, 1237.

43. K. Xiao, L. X. Ding, G. X. Liu, H. B. Chen, S. Q. Wang and H. H. Wang, *Adv. Mater.*, 2016, **28**, 5997.

44. L. F. Shen, L. Yu, H. B. Wu, X. Y. Yu, X. G. Zhang and X. W. Lou, *Nat. Commun.*, 2015, **6**, 6694.

45. L. L. Li, S. J. Peng, H. B. Wu, L. Yu, S. Madhavi and X. W. Lou, *Adv. Energy Mater.*, 2015, **5**, 1500753.

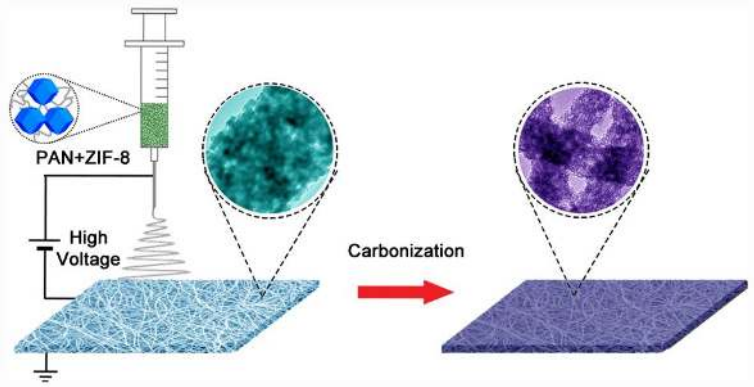

Fig. 1 Schematic illustration of the synthesis of hollow particle-based N-doped carbon nanofibers (HPCNFs-N).

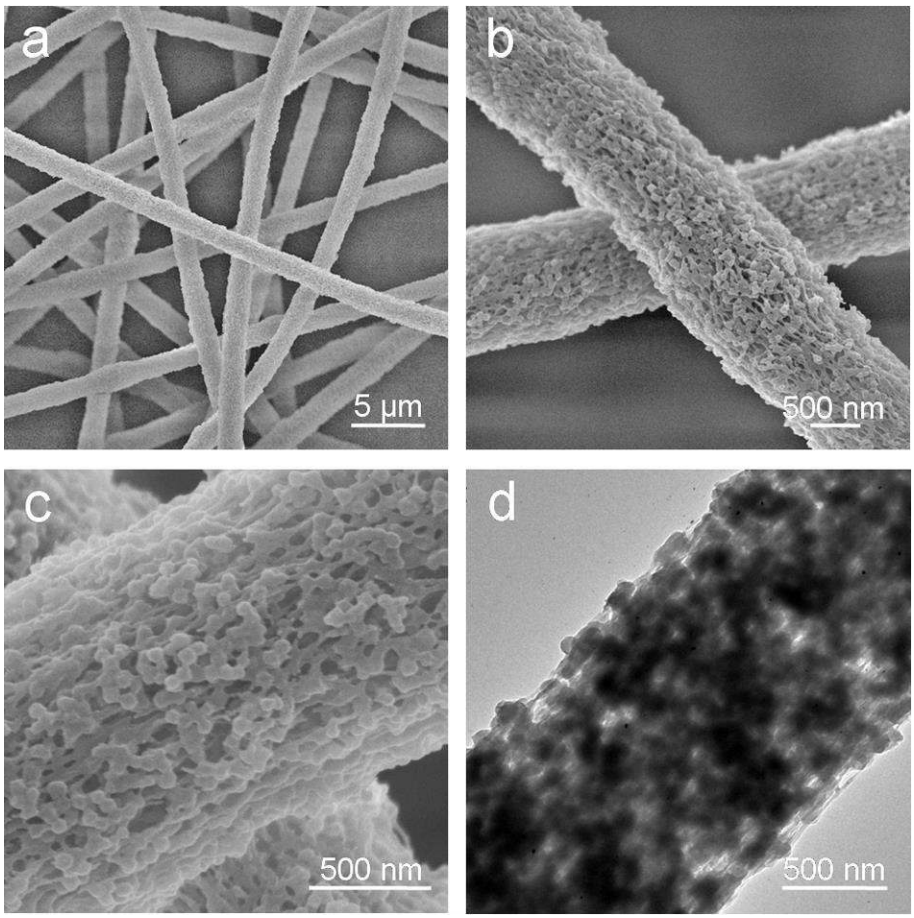

Fig. 2 FESEM and TEM images of the PAN/ZIF-8 composite nanofibers.

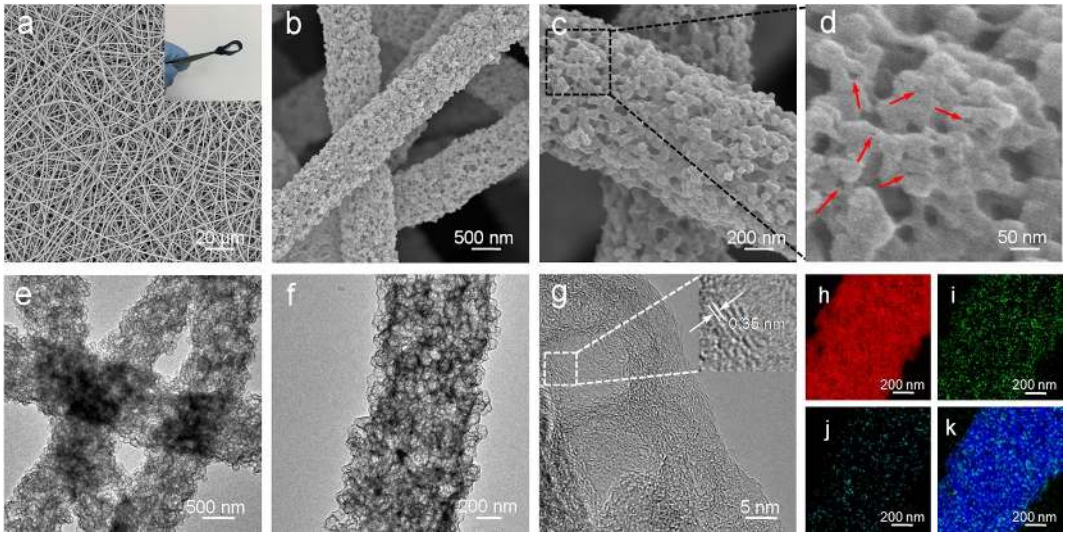

Fig. 3 FESEM and TEM images of the HPCNFs-N sample. (a-c) Top view of FESEM images; (d) magnified FESEM image of the selected region in (c); (e and f) TEM and (g) HRTEM images. Elemental mapping images of (h) C, (i) N, (j) O and (k) overlap. Inset in (a): photograph of a piece of folded HPCNFs-N sample. Inset in (g): a high resolution TEM image of the HPCNFs-N shell.

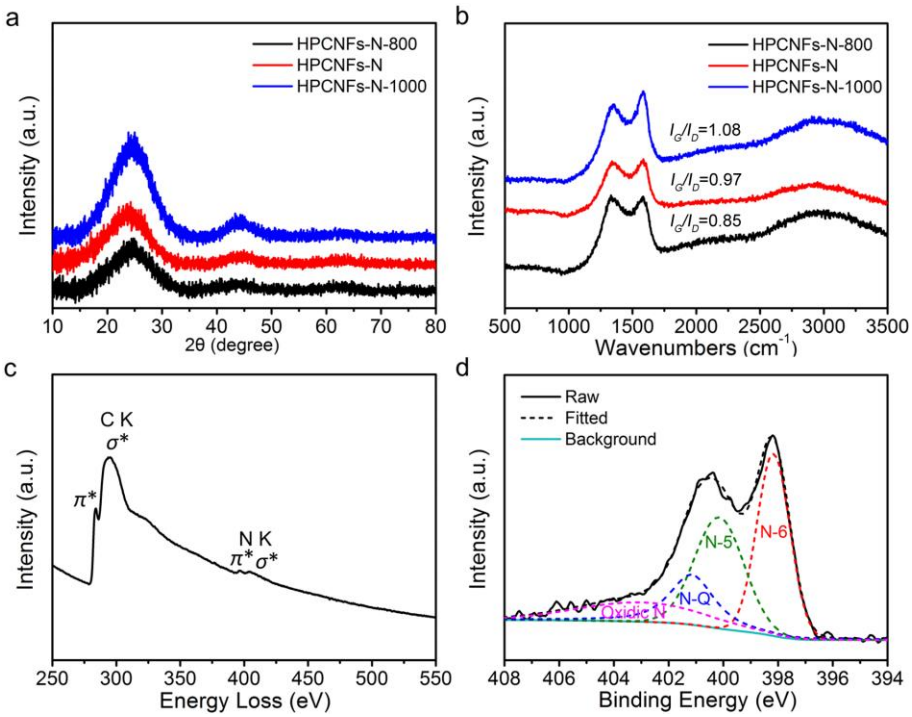

Fig. 4 (a) XRD patterns and (b) Raman spectra of HPCNFs-N and the control samples. (c) Electron energy loss spectroscopy and (d) high-resolution XPS spectra of deconvoluted N1s peak of the HPCNFs-N sample.

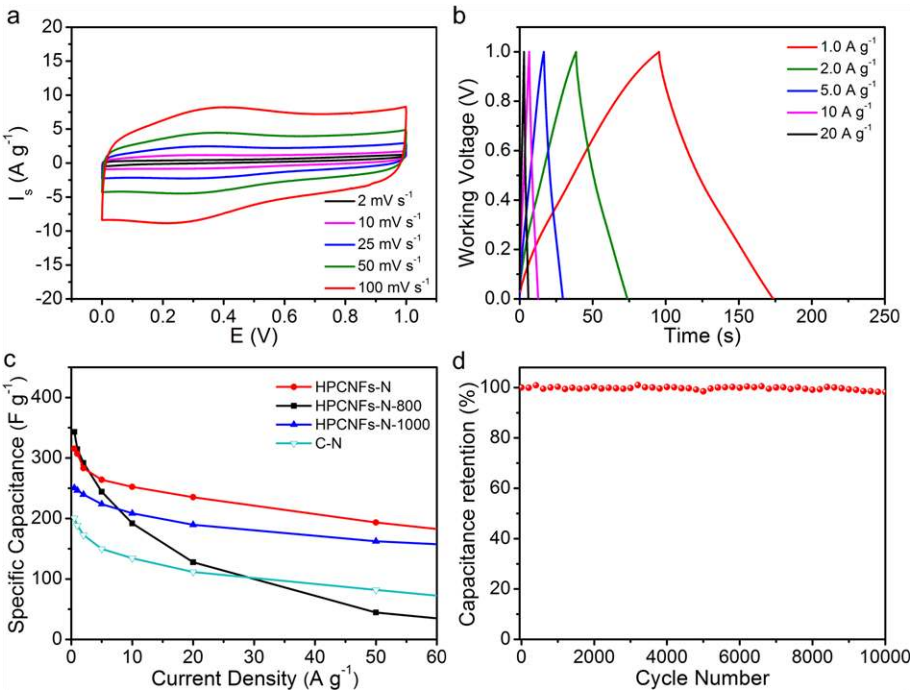

Fig. 5 (a) CV curves of the HPCNFs-N sample at different scan rates. (b) Galvanostatic charge-discharge curves at different current densities and (c) variation of specific capacitance against the current density of HPCNFs-N and the control samples. (d) Cycling performance of the HPCNFs-N device at a current density of 5.0 A g^{-1}.

For Table of Contents Use

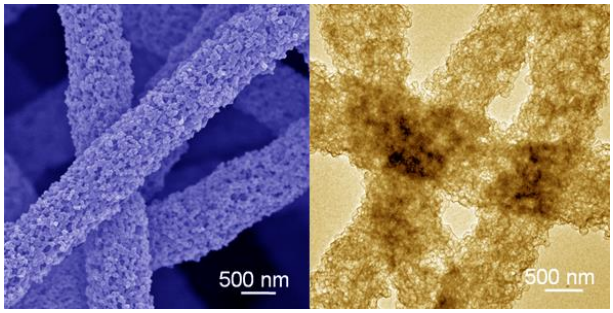

Hollow particle-based N-doped carbon nanofibers synthesized by a facile electrospinning and carbonization method exhibit enhanced supercapacitive performance.